

Intervessel pit membrane thickness best explains variation in embolism resistance amongst stems of *Arabidopsis thaliana* accessions

Ajaree Thonglim^{1*}, Sylvain Delzon², Maximilian Larter¹, Omid Karami³, Arezoo Rahimi³, Remko Offringa³, Joost J. B. Keurentjes⁴, Salma Balazadeh³, Erik Smets¹, and Frederic Lens^{1*}

¹Naturalis Biodiversity Center, Research Group Functional Traits, PO Box 9517, 2300 RA Leiden, The Netherlands; ²BIOGECO INRA, Université Bordeaux, 33615 Pessac, France;

³Plant Developmental Genetics, Institute of Biology Leiden, Leiden University, 2333 BE Leiden, the Netherlands; ⁴Laboratory of Genetics, Wageningen University, Droevendaalsesteeg 1, 6708 PB Wageningen, The Netherlands.

*For correspondence. E-mail ajaree.thonglim@naturalis.nl; frederic.lens@naturalis.nl

© The Author(s) 2020. Published by Oxford University Press on behalf of the Annals of Botany Company.

This is an Open Access article distributed under the terms of the Creative Commons Attribution License (<http://creativecommons.org/licenses/by/4.0/>), which permits unrestricted reuse, distribution, and reproduction in any medium, provided the original work is properly cited.

- **Background and Aims** The ability to avoid drought-induced embolisms in the xylem is one of the essential traits for plants to survive periods of water shortage. Over the past three decades, hydraulic studies have been focusing on trees, which limits our ability to understand how herbs tolerate drought. Here, we investigate the embolism resistance in inflorescence stems of four *Arabidopsis thaliana* accessions that differ in growth form and drought response. We assess functional traits underlying the variation in embolism resistance amongst the accessions studied using detailed anatomical observations.
- **Methods** The vulnerability to xylem embolism was obtained via vulnerability curves using the centrifuge technique and linked with detailed anatomical observations in stems using light microscopy and transmission electron microscopy.
- **Key results** The data show significant differences in stem P_{50} , varying twofold from -1.58 MPa in the Cape Verde Island accession to -3.07 MPa in the woody *soc1 ful* double mutant. Out of all the anatomical traits measured, intervessel pit membrane thickness (T_{PM}) best explains the differences in P_{50} , as well as P_{12} and P_{88} . The association between embolism resistance and T_{PM} can be functionally explained by the air-seeding hypothesis. There is no evidence that the correlation between increased woodiness and increased embolism resistance is directly related to functional aspects. However, we found that increased woodiness is strongly linked to other lignification characters, explaining why mechanical stem reinforcement is indirectly related to increased embolism resistance.

- **Conclusions** The woodier or more lignified accessions are more resistant to embolism than the herbaceous accessions, confirming the link between increased stem lignification and increased embolism resistance as also observed in other lineages. Intervessel pit membrane thickness, and to a lesser extent theoretical vessel implosion resistance and vessel wall thickness, are the missing functional links between stem lignification and embolism resistance.

Key words: *Arabidopsis thaliana*, embolism resistance, herbaceous species, intervessel pit membrane, lignification, stem anatomy, xylem hydraulics.

Accepted Manuscript

INTRODUCTION

Long-distance water transport in the xylem connecting roots to leaves is essential for plant survival and distribution (Sperry, 2003; Brodribb, 2009; Lucas *et al.*, 2013; Lens *et al.*, 2016; Trueba *et al.*, 2017; Choat *et al.*, 2018; Brodribb *et al.*, 2020). Plants have developed an ingenious system to transport water upwards against gravity by a largely passive mechanism that is driven by a difference in negative xylem pressure created in the leaf mesophyll cell walls, known as the cohesion-tension theory (Dixon and Joly, 1895; Pickard, 1981; Brown, 2013). However, this negative or subatmospheric pressure inside the water-conducting xylem conduits puts water in a metastable liquid state, making it vulnerable to heterogeneous cavitation: the transition from liquid water to vapour by spontaneous destabilization of the hydrogen bonds between water molecules at nucleating sites (Steudle, 2001; Wheeler and Stroock, 2008; Brown, 2013; Venturas *et al.*, 2017). Under drought stress conditions, the xylem pressure becomes more negative, thereby increasing the risk of tiny vapour bubbles enlarging into a large embolism that blocks the water transport inside a conduit (Sperry and Tyree, 1988; Tyree and Zimmermann, 2002; Cochard, 2006). This embolized conduit can then cause gas bubbles to spread towards adjacent water-filled conduits via tiny pores in the interconduit pit membranes, a process called air-seeding. Air-seeding may lead to a rapid spread of drought-induced embolism throughout the plant, giving rise to hydraulic failure, i.e. a catastrophic loss of xylem hydraulic conductance, ultimately causing plant death (Brodribb and Cochard, 2009; Allen *et al.*, 2010; Urli *et al.*, 2013; Brodribb *et al.*, 2016, 2020; Anderegg *et al.*, 2016; Adams *et al.*, 2017; Kaack *et al.*, 2019; Zhang *et al.*, 2020). Acquiring a sufficient level of embolism resistance, therefore, represents one of the most essential adaptations for plant survival under drought conditions, along with other strategies such as reduced water-loss, increased water storage or root depth (Lens *et al.*, 2013; Gleason *et al.*, 2014; Martin-StPaul *et al.*, 2017; Billon *et al.*, 2020).

The relationship between the decline in hydraulic conductivity due to embolism and xylem pressure is plotted in a so-called vulnerability curve (VC), from which the pressure

inducing 50% loss of hydraulic conductivity (P_{50}) – the often-cited proxy for drought tolerance – is derived (Maherali *et al.*, 2004; Choat *et al.*, 2012; Venturas *et al.*, 2017). Hydraulic studies show a wide range of P_{50} across species (from -0.5 MPa to -20 MPa), and species occupying dry habitats are generally more resistant to embolism formation (more negative P_{50}) than species from wet habitats (Brodribb and Hill, 1999; Choat *et al.*, 2012; Larter *et al.*, 2015; Lens *et al.*, 2016; Trueba *et al.*, 2017). Xylem physiologists have measured P_{50} values in stems of over 2000 tree and shrub species. However, hydraulic measurements in herbaceous species are limited to only a few dozen species, despite the fact that a majority of our important food crops are herbs (Stiller, 2002; Holloway-Phillips and Brodribb, 2011; Lens *et al.*, 2013, 2016; Nolf *et al.*, 2016; Skelton *et al.*, 2017; Ahmad *et al.*, 2018; Dória *et al.*, 2018; Volaire *et al.*, 2018; Lamarque *et al.*, 2020; Bourbia *et al.*, 2020; Corso *et al.*, 2020). Therefore, it is essential to focus more on herb hydraulics and integrate these hydraulic traits in models that predict annual crop yields to consider the effects of drought and heatwave events (Asseng *et al.*, 2015).

In this paper, we focus on the model species *Arabidopsis thaliana* (L.) Heynh. This small herbaceous species is able to produce a limited amount of wood in the hypocotyl and at the base of the inflorescence stem (Chaffey *et al.*, 2002; Ko *et al.*, 2004; Nieminen *et al.*, 2004; Melzer *et al.*, 2008; Lens *et al.*, 2012). Wood formation can be moderately induced in wildtype accessions by either delaying flowering time under short days (Tixier *et al.*, 2013) or by clipping developing flowers (Chaffey *et al.*, 2002), by applying weights on the inflorescence stem (Ko *et al.*, 2004), or by increasing auxin levels (Agusti *et al.*, 2011; Brackmann *et al.*, 2018). A more extensive wood cylinder can be induced by modifying gene regulation that turns the herbaceous phenotype into a shrubby phenotype (Melzer *et al.*, 2008; Karami *et al.*, 2020), although this woodiness does not extend towards the upper parts of the inflorescence stems (Lens *et al.*, 2012). Since increased woodiness or lignification levels in stems have been linked to higher levels of embolism resistance in various plant groups (Tixier *et al.*, 2013; Lens *et al.*, 2013, 2016; Dória *et al.*, 2018, 2019), we selected three

herbaceous wildtype accessions of *A. thaliana* with a different growth type and drought response (Columbia (Col-0), Cape Verde Islands (Cvi) and Shahdara (Sha); Bac-Molenaar *et al.*, 2016; Thoen *et al.*, 2017) and one woody mutant established in the Col-0 background (*soc1 ful* knockout; Melzer *et al.*, 2008) to evaluate this potential correlation more closely. To this end, we applied the cavitron centrifuge method (Cochard *et al.*, 2013) to compare the xylem embolism resistance of inflorescence stems amongst the four accessions, and assessed which xylem anatomical traits underlie the differences observed in P_{50} using detailed anatomical observations with light microscopy (LM) and transmission electron microscopy (TEM). Various hydraulically relevant stem traits were observed, such as the proportion of stem woodiness/lignification, intervessel pit membrane thickness, fibre wall thickness, theoretical vessel implosion index, and vessel grouping index (Table 1). We hypothesize that woodier or more lignified *Arabidopsis* stems are more resistant to embolism formation than less lignified stems and that this difference in embolism resistance is functionally driven by intervessel pit membrane thickness.

MATERIALS AND METHODS

Plant material

Three accessions and one woody mutant of *Arabidopsis thaliana* were chosen based on their contrasting growth form, the difference in drought tolerance and the minimum length of their inflorescence stems: (1) Columbia (Col-0, a direct descendant of Col-1 from Poland and Eastern Germany; Koornneef and Meinke, 2010; Passardi *et al.*, 2007; Somssich, 2019); (2) Shahdara (Sha, native to a low precipitation area of Shakhdarah valley, Tajikistan; Khurmatov, 1982; Trontin *et al.*, 2011); (3) Cape Verde Islands (Cvi, native to the high altitude region above 1,200 m on Cape Verde Islands; (Lobin, 1983; Monda *et al.*, 2011); and (4) Col-0 accession in which two flowering time control genes SUPPRESSOR OF OVEREXPRESSION OF CO 1 (SOC1) and FRUITFULL (FUL) are knocked out (*soc1 ful* in Col-0 background; (Melzer *et al.*, 2008). The three wildtype accessions were selected based

on the length of their inflorescence stems (at least 30 cm required for the cavitron measurements, which exceeds by far the maximum vessel length of Col-0 reaching only 4 cm according to Tixier *et al.* (2013), to avoid potential open-vessel artefacts (Cochard *et al.*, 2013)), their differences in drought response (Bac-Molenaar *et al.*, 2016; Thoen *et al.*, 2017) and growth form. The *soc1 ful* knockout was selected as the woody counterpart because of its extended levels of wood formation at the base of the inflorescence stems (Lens *et al.*, 2012). One hundred individuals from three accessions and one double knockout were grown from seeds sown directly in a mixture of soil and sand (4.5:1). After seed germination (10-12 days after sowing), the healthy seedlings were transferred and grown individually in 8 cm-diameter pots in a growth chamber under controlled conditions of 20°C temperature and 16-h photoperiod, with 100 $\mu\text{mol m}^{-2} \text{s}^{-1}$ light intensity. Relative humidity (RH) was maintained at 70%. We synchronized the harvesting time for the four accessions, meaning that each accession was harvested at different ages (55-65 days for WT accessions, 80-90 days for *soc1 ful*), depending on the time required for flowering and inflorescence stem development.

Xylem vulnerability to embolism

Sample preparation of inflorescence stems The plants were harvested – with roots, leaves and flowers still attached – in the growth chamber facilities at the Institute of Biology Leiden (Leiden University, The Netherlands). The basal part of the inflorescence stems of each accession was cut underwater with a sharp razor blade into a length at least of 30 cm, and then immediately wrapped in wet tissues, enclosed in plastic bags, and shipped to the PHENOBOIS platform (INRAE, University of Bordeaux, France) for the hydraulic experiments that were carried out within a week of harvest. Before running the cavitron centrifuge measurements, the samples were recut underwater to a standard length of 27 cm, after which both ends were trimmed to fit the cavitron rotor. All siliques, leaves and flowers were removed from the stems just before the measurement.

Cavitron centrifuge method

Centrifugal force has been used to induce cavitation in stem segments by lowering the xylem pressure in the middle part of stems during spinning (Cochard, 2002; Cochard *et al.*, 2005). Vulnerability to embolism in the inflorescence stems was measured using ten individuals per vulnerability curve (VC) to generate sufficient hydraulic conductivity during the spinning experiment; about 10 VCs per accession were generated. A solution of deionized ultrapure water containing 1 mM CaCl₂ and 10mM KCl was used as a reference for the hydraulic conductivity measurements. The theoretically maximum hydraulic conductivity (K_{max} , m² MPa⁻¹ s⁻¹) of the ten inflorescence stems was firstly calculated at near-zero MPa (low speed). The xylem pressure was then gradually decreased by -0.2 to -0.4 MPa for each spinning step. The hydraulic conductivities at every rotation speed (K) were measured using Cavisoft software (Cavisoft v1.5, University of Bordeaux, France). The percentage loss of hydraulic conductivity (PLC) was computed as:

$$PLC = 100 \cdot (1 - (K/K_{MAX})) \quad (1)$$

The vulnerability curves were constructed and fitted with a sigmoid function (Pammenter and Van der Willigen, 1998) using NLIN procedure in SAS 9.4 (SAS 9.4; SAS Institute, Cary, NC, USA) following the equation:

$$PLC = 100 / [1 + \exp ((S/25) \cdot (P - P_{50}))] \quad (2)$$

where P_{50} represents the xylem pressure inducing 50% loss of hydraulic conductivity and S (% MPa⁻¹) is the slope of the VC at the inflexion point (P_{50}).

Stem anatomy

Sample preparation Since the stem anatomy at the basal, more lignified part differs rather considerably compared to the middle part where the negative pressures were applied during the cavitron measurements, we made sections from both parts and performed the anatomical observations on the middle stem parts to match anatomy with P_{50} . From the 10 VCs we generated per accession, we selected three stems for three representative VCs (9 individuals per accession) for light microscopy (LM), and one stem for three representative VCs (3 individuals per accession) for transmission electron microscopy (TEM). The anatomical measurements (Table 1) were carried out using ImageJ (National Institutes of Health, Bethesda, USA) following the recommendations of (Scholz *et al.*, 2013).

Light microscopy (LM)

The inflorescence stems were cut into small pieces, ca 1 cm long and stored in 70% ethanol. Fixed samples were then infiltrated and embedded in LR-White resin (Hamann *et al.*, 2011). The embedded samples were sectioned using a Leica RM 2265 microtome with disposable Tungsten carbon blades (Leica, Eisenmark, Wetzlar, Germany) at a thickness of 4 μm . Subsequently, the sections were heat-fixed onto the slides with 40% acetone, stained with Toluidine blue (1% (w/v) toluidine blue (VWR chemical BDH®, Radnor, Pennsylvania, USA) in 1% (w/v) borax), rinsed with distilled water, air-dried, and mounted with DPX new-100579 mounting medium (Merck Chemicals B.V., Amsterdam, Northern Holland, The Netherlands). The anatomical features were observed under a Leica DM2500 light microscope and photographed with a Leica DFC-425 digital camera (Leica microscopes, Wetzlar, Germany). The diameter of vessels (D) was calculated as:

$$D = (\sqrt{4A}) / \pi \quad (3)$$

where D represents the diameter of vessels, and A is the conduit surface area. The hydraulically weighted vessel diameter (D_H) was calculated based on the diameter of vessels (D) following the equation (Tyree and Zimmermann, 2002):

$$D_H = (\sum D^4 / N)^{1/4} \quad (4)$$

where D is the diameter of vessels measured using equation 3 and N is the number of conduits measured. All the measurements are explained in Table 1.

Transmission Electron Microscopy (TEM)

After the cavitron experiment, 1 cm-long pieces from the middle part of the inflorescence stems were immediately collected and fixed in Karnovsky's fixative for 48 hr (Karnovsky, 1965). The samples were cleaned three times in 0.1M cacodylate buffer, then post-fixed with 1% buffered osmium tetroxide, rinsed again with buffer solution, stained with 1% uranyl acetate, and dehydrated in a series of ethanol: 1 % uranyl acetate replacement, with increasing concentration of ethanol (30%, 50%, 70%, 96%, and twice in $\geq 99\%$). The samples were then infiltrated with Epon 812 n (Electron Microscopy Sciences, Hatfield, England) and placed at 60°C for 48 hr in the oven. The Epon blocks were trimmed into 2 μm -thick using rotary microtome with a glass knife. Subsequently, the cross-sections with many vessel-vessel contact areas were cut into ultrathin sections of 90-95 nm using a Leica EM UC7 ultramicrotome with a diamond knife. The sections were dried and mounted on film-coated copper slot grids with Formvar coating (Agar Scientific, Stansted, UK), and post-stained with uranyl acetate and lead citrate. Ultrastructural observations of intervessel pits were performed and photographed using a JEM-1400 Plus TEM (JEOL, Tokyo, Japan), equipped with an 11 MPixel camera (Quemesa, Olympus). At least 25 relaxed, non-shrunken intervessel pit membranes

were selected from 3 individuals per accession to observe intervessel pit membranes thickness and pit chamber depth (Table 1).

Statistical analysis

To assess the differences between embolism resistance among the four accessions studied, we performed General Linear Models (GLM). A Newman-Keuls post-hoc test was applied to test whether or not embolism resistance (P_{50}) and anatomical characters differ amongst accessions. We carried out multiple linear regression models based on non-standardized and standardized data from the middle part of the stem segments to evaluate which stem anatomical traits (predictive variables) best explain embolism resistance, with P_{50} , P_{12} (air entry point) and P_{88} as response variables. Predictors were firstly selected based on biological knowledge, followed by a collinearity analysis through pairwise scatterplots and variance inflation factor (VIF). To deduce the most parsimonious multiple linear regression model, we applied “step” function from “stats” package (R Core Team 2016; available in CRAN) to remove the least predictive variables each time according to Akaike Information Criterion (AIC). Robust fitting of linear models through iteratively reweighted least squares (IWLS) and MM estimation (M-estimation with Tukey’s bi-weight initialized by a specific S-estimator) was used to deal with the outliers and leverages.

In addition, to assess the relative importance of the remaining explanatory variables of P_{50} , we calculated the relative importance of regressors in linear models. Pearson’s correlation analysis was applied to assess the correlation between the predictive variables and P_{50} . We used R version 3.6.3 in R Studio version 1.2.5033 for all analyses. All the differences were considered significant when p-value was <0.05.

RESULTS

Xylem vulnerability to embolism amongst the Arabidopsis accessions

P_{50} of each accession is significantly different from each other and varied twofold across the accessions studied ($F = 57.70$; $p\text{-value} < 0.001$) from -1.58 MPa to -3.07 MPa (Fig. 1). Amongst the four accessions, stems of the *soc1 ful* double mutant are the most resistant to embolism ($P_{50} = -3.07 \pm 0.30$ (SD) MPa; Supplementary Data Table S1) with a slope of 62% MPa⁻¹ (Fig. 1a), followed by Sha ($P_{50} = -2.49 \pm 0.11$ MPa; slope = 59% MPa⁻¹), Col-0 ($P_{50} = -2.14 \pm 0.18$ MPa; slope = 38% MPa⁻¹), and Cvi ($P_{50} = -1.58 \pm 0.05$ MPa; slope = 142% MPa⁻¹) (Supplementary Data Table S1; Fig. 1a). The P_{50} variation within accessions is remarkably low except for *soc1 ful* ranging from -2.59 MPa to -3.42 MPa (Fig. 1b). Similar significant variation in P_{12} ($F = 26.79$; $p\text{-value} < 0.001$) is observed; for P_{88} , Col-0 and Sha are not significantly different from each other ($F = 34.8$; $p\text{-value} = 0.517$).

Stem anatomical traits amongst the accessions studied

The features that are significantly different from each other among the accessions studied are intervessel pit membrane (T_{PM}) ($F = 118.8$; $p\text{-value} < 2e^{-16}$; Supplementary Data Fig. S1a; Figs 2c-d; Figs 3c-d), theoretical vessel implosion resistance (T_{VW}/D_{MAX})² ($F = 37.35$; $p\text{-value} = 1.44e^{-10}$; Supplementary Data Fig. S1b) and proportion of fibre wall area per fibre cell area (P_{FWFA}) ($F = 65.33$; $p\text{-value} = 9.75e^{-14}$; Supplementary Data Fig. S1c). Meanwhile, proportion of lignified area per total stem area (P_{LIG}) of Col-0 is different from *soc1 ful* and Cvi ($F = 18.68$; $p\text{-value} = 3.48e^{-07}$; Supplementary Data Fig. S1d), which is similar to Sha. Furthermore, vessel grouping index (V_G) of Col-0 and Cvi is similar, which is also the case for Sha and *soc1 ful*; V_G of both groups, however, are significantly different from each other ($F = 43.45$; $p\text{-value} = 2.17e^{-11}$; Supplementary Data Fig. S1e). Vessel wall thickness (T_V) of Col-0 and Cvi are different from each other, and different from Sha and

soc1 ful which have a similar T_V ($F = 33.46$; $p\text{-value} = 5.52e^{-10}$; Supplementary Data Fig. S1f).

Relationship between embolism resistance and anatomical features

Both T_{PM} and $(T_{VW}/D_{MAX})^2$ strongly correlated positively with embolism resistance based on a Pearson correlation test ($r = -0.93$, $p\text{-value} = 3.1e^{-16}$; $r = -0.88$, $p\text{-value} = 2.1e^{-12}$, respectively; Figs. 4b-c). Furthermore, there are correlations between embolism resistance and vessel wall thickness (T_V) ($r = -0.86$, $p\text{-value} = 2.5e^{-11}$; Supplementary Data Fig. S2a), between embolism resistance and vessel grouping index (V_G) ($r = -0.77$, $p\text{-value} = 3.6e^{-08}$; Supplementary Data Fig. S2b)), between embolism resistance and proportion of lignified area per total stem area (P_{LIG}) ($r = -0.67$, $p\text{-value} = 7.2e^{-06}$; Supplementary Data Fig. S2c), and between embolism resistance and proportion of fibre wall per fibre cell area (P_{FWFA}) ($r = -0.73$, $p\text{-value} = 3.4e^{-07}$; Supplementary Data Fig. S2d).

Multiple regression analysis with robust fitting shows that the best predictors explaining P_{50} variation are thickness of intervessel pit membrane (T_{PM} ; Figs. 2c-d, 3c-d) and theoretical vessel implosion resistance ($(T_{VW}/D_{MAX})^2$), followed by vessel wall thickness (T_V), and vessel grouping index (V_G) ($R^2 = 0.9468$ $p\text{-value} < 2.2e^{-16}$) (Table 2). However, only T_{PM} and $(T_{VW}/D_{MAX})^2$ are highly significant in this model ($p\text{-value} < 0.01$) (Table 2). According to the regressor analysis, the relative importance of T_{PM} and $(T_{VW}/D_{MAX})^2$ in explaining P_{50} variation is 31% and 25%, respectively (Table 2, Fig. 4a). The proportion of lignified area per total stem area (P_{LIG}) does not explain embolism resistance based on the most parsimonious multiple regression model (AIC score = -134.39; Table 2, Supplementary Data Table S2), but is included in the second most parsimonious model (AIC = -132.44; Supplementary Data Table S3).

Correspondingly, T_{PM} also best explains P_{12} and P_{88} variations based on multiple regression models, followed by pit chamber depth (D_{PC}) ($R^2 = 0.9507$ $p\text{-value} < 2.2e^{-16}$, $R^2 =$

0.8646 p-value $<3.88e^{-13}$, respectively) (Supplementary Data Tables S4, S5). In addition, theoretical vessel implosion resistance $((T_{VW}/D_{MAX})^2)$ is included in P_{88} multiple regression model (p-value <0.05) (Supplementary Data Tables S5), while T_V is included in the P_{12} multiple regression model as a significant predictor (p-value < 0.001) (Supplementary Data Tables S4).

Correlations between the anatomical variables are the following: thickness of intervessel pit membrane is strongly correlated to theoretical vessel implosion resistance, vessel wall thickness, vessel grouping and proportion of fibre wall per fibre cell area ($r = 0.77, 0.76, 0.72$ and 0.68 , respectively; p-value <0.001) (Supplementary Data Fig. S3). Apart from that, $(T_{VW}/D_{MAX})^2$ correlates with T_V , V_G and P_{FWFA} ($r = 0.77, 0.62$ and 0.59 , p-value <0.001), V_G is correlated with T_V ($r = 0.63$; p-value <0.001) (Supplementary Data Fig. S3), and P_{LIG} shows correlations with T_{PM} , V_G , $(T_{VW}/D_{MAX})^2$ and T_V ($r = 0.67, 0.66, 0.58$ and 0.58 , respectively; p-value <0.001 ; Supplementary Data Fig. S3).

DISCUSSION

We found twofold variation in stem P_{50} amongst the *Arabidopsis thaliana* accessions studied (ranging from -1.5 to -3.0 MPa; Fig. 1), which is significantly associated with an increase in the thickness of the intervessel pit membrane (T_{PM} ; Fig. 4) and is in line with the air-seeding hypothesis. Our findings confirm earlier reports that *Arabidopsis* inflorescence stems with increased levels of lignification are better able to avoid drought-induced embolism than stems that are less lignified (Figs. 2-3), which is based on (1) a more elaborate set of wildtype accessions (three vs one), (2) multiple vulnerability curves (VCs) per accession compared to only one VC per accession, and (3) more detailed anatomical observations compared to previous structure-function papers in *Arabidopsis* (Lens *et al.*, 2013; Tixier *et al.*, 2013). We investigated correlations amongst a range of anatomical traits related to stem lignification and uncovered statistical associations between increased lignification vs T_{PM} and between vessel wall thickness vs T_{PM} . Our comparative approach

suggests an indirect link between traits related to mechanical strength in stems and P_{50} , with T_{PM} serving as the missing functional link between stem reinforcement and vulnerability to embolism.

Variation in stem P_{50} amongst Arabidopsis accessions agrees with other herbs and is best explained by intervessel pit membrane thickness (T_{PM})

Our embolism resistance measurements with the cavitron technique support earlier papers reporting values for the same species based on the more traditional centrifuge technique in combination with a portable water flow device (XYL'EM) (from -2.25 to -3.5 MPa; Lens *et al.*, 2013; Tixier *et al.*, 2013). Our data also fall within the range of the published P_{50} values for herbaceous eudicot species (Tyree *et al.*, 1986; Stiller, 2002; Saha *et al.*, 2009; Li *et al.*, 2009; Rosenthal *et al.*, 2010; Nolf *et al.*, 2014; Skelton *et al.*, 2017; Dória *et al.*, 2018, 2019; Bourbia *et al.*, 2020), although more negative P_{50} values (up to -7.5 MPa) of herbaceous stems, especially in grasses, have been reported in some papers (Lens *et al.*, 2016; Volaire *et al.*, 2018).

Amongst the anatomical traits we observed, T_{PM} strongly correlates with P_{50} and explains best the variation in P_{50} observed based on a statistical test showing the relative importance of regressors in our most parsimonious multiple linear regression model (Table 2; Figs. 4a-b). Our observations in *Arabidopsis* fit well with other published data of woody and herbaceous species where properly fixated intervessel pit membranes have been measured in stems that were subjected to P_{50} measurements (Li *et al.*, 2016; Dória *et al.*, 2018, 2019; Supplementary Data Fig. S4). Furthermore, intervessel pit membrane thickness is the only trait that is also significant in the P_{12} and P_{88} multiple regression models, which emphasizes the functional relevance of T_{PM} in our dataset (Supplementary Data Tables S4, S5). As highlighted before, this T_{PM} - P_{50} correlation is undoubtedly functionally relevant because it nicely fits with the air-seeding mechanism. Although we do not fully understand exactly how this mechanism works at the ultrastructural level, the oversimplified 2D view suggesting that

air-seeding occurs via the single largest pit membrane pore should be abandoned (Wheeler *et al.*, 2005). Instead, a more realistic 3D structure of intervessel pit membranes shows that a single pit membrane pore – being highly interconnected with other pores – has multiple constrictions that are often narrower than 50 or 20 nm when pit membranes are thinner or thicker than 300 nm, respectively (Zhang *et al.*, 2020). In other words, the chance of having a smaller pore constriction becomes higher with thicker pit membranes as this elongates the multiconstriction pit membrane pore. Consequently, air-seeding is not determined by the single largest pore in a pit membrane, but by the minimum constriction across all the interconnected pores in a given pit membrane (Kaack *et al.*, 2019; Zhang *et al.*, 2020). This explains why species with thicker intervessel pit membranes are better able to withstand air bubble spread between adjacent conduits under drought conditions than species with thinner intervessel pit membranes (Jansen *et al.*, 2009; Li *et al.*, 2016; Dória *et al.*, 2018). However, more ultrastructural observations of intact pit membranes and the role of surface-active substances such as phospholipids in the xylem sap and pit membranes should be carried out to improve our understanding of air bubble formation and spread at the ultrastructural level (Schenk *et al.*, 2017, 2018; Zhang *et al.*, 2020).

Disentangling the correlation between traits impacting mechanical strength and embolism resistance

Based on Pearson's correlation test, the proportion of lignified area per total stem area (P_{LIG}) is significantly correlated to P_{50} (Supplementary Data Figs. S2c, S3). This is in line with our previous results in *Arabidopsis* (Lens *et al.*, 2013), in other lineages of Brassicaceae and Asteraceae (Dória *et al.*, 2018, 2019), and in grasses (Lens *et al.*, 2016) showing that more woody/lignified stems are more resistant to embolism formation compared to close relatives with less woody/lignified stems. However, P_{LIG} is not included in the most parsimonious multiple regression P_{50} model (Table 2); it is retained in the second most

parsimonious model (Supplementary Table S3), though, explaining only 10% of the P_{50} variation (results not shown). Consequently, in our dataset, P_{LIG} is not a key functional trait contributing to vulnerability to embolism in stems of the *Arabidopsis* accessions studied. Still, it does have predictive value due to its correlation with other traits that are considered to be more relevant.

Interestingly, P_{LIG} is significantly correlated to several other lignification traits, of which intervessel pit membrane thickness (T_{PM}), theoretical vessel implosion resistance (T_{VW}/D_{MAX})² and vessel wall thickness (T_V) are prime examples (Supplementary Data Fig. S3). These three traits explain altogether, 79% of the P_{50} variation in the most parsimonious multiple regression model (Fig. 4a). When comparing the three P_{12} - P_{50} - P_{88} multiple regression models, it is interesting to note that the depth of pit chamber (D_{PC}) is absent in the P_{50} model (Table 2) but pops up as highly significant in both P_{12} - P_{88} models (Supplementary Data Tables S4, S5). It is hypothesized that shallower pit chambers minimize interconduit pit membrane stretching during aspiration and thereby reducing the mechanical stresses on the membranes in both angiosperms as gymnosperms (Hacke and Jansen, 2009; Lens *et al.*, 2011). However, D_{PC} does not seem to be generally correlated with embolism resistance across all lineages observed (Dória *et al.*, 2018).

The (indirect) correlation between P_{50} and traits impacting mechanical strength has also been highlighted in other studies that have found links between embolism resistance vs thickness-to-span ratio of conduits (Hacke *et al.*, 2001; Bouche *et al.*, 2014), vs vessel wall thickness (Jansen *et al.* 2009; Li *et al.* 2016; see also next paragraph), vs wood density (Jacobsen *et al.*, 2005; Hoffmann *et al.*, 2011; Anderegg *et al.*, 2016; Gleason *et al.*, 2016), vs fibre wall thickness (Jacobsen *et al.*, 2005, 2007), vs lignin content (Pereira *et al.*, 2018), and vs lignin composition (Awad *et al.*, 2012; Lima *et al.*, 2018). Out of all these lignification characters, vessel wall reinforcement for a given lumen area – expressed either as thickness-

to-span ratio of vessels or theoretical vessel implosion resistance – explains 25% of the P_{50} variation (Fig. 4a), but only 3% of the P_{88} variation (results not shown), and could potentially present a secondary functional link due to its direct association with the long-distance water flow in plants that is prone to negative pressures. Also, in conifers, the pressure causing conduit implosion is correlated with embolism resistance, but it is more negative than P_{50} for most species. Since vessel collapse due to negative pressures has never been observed in woody nor herbaceous stems, it suggests that embolism occurs before the critical vessel implosion threshold is reached (Choat *et al.*, 2012; Bouche *et al.*, 2014), which is likely also the case for herbaceous species. Only a few reports of (reversible) vessel collapse in the smallest leaf veins are reported, which could be a mechanism to prevent embolism upstream in the major veins (Zhang *et al.*, 2016).

Variation in theoretical vessel implosion resistance $((T_{VW}/D_{MAX})^2)$ among *Arabidopsis thaliana* stems studied is mainly determined by the changes of vessel wall thickness (T_V), explaining 64% of the variation, whereas, the maximum vessel lumen diameter (D_{MAX}) only accounts for 31% (Supplementary Figure S5). This result is in line with Bouche *et al.* (2014), who found that T_V drives the variation in T_{VW}/D_{MAX} , suggesting that species tend to mechanically reinforce their conduits by increasing wall thickness instead of reducing conduit size in order to maintain a minimum level of hydraulic conductance. But, at the same time, T_V also positively correlates with T_{PM} (Supplementary Data Fig. S3), with thicker vessel walls leading to thicker intervessel pit membranes (Jansen *et al.*, 2009) and thus higher embolism resistance (T_V explaining 23% of the P_{50} variation (Fig. 4a) and 18% of the P_{12} variation (results not shown)). On the other hand, other studies investigating the driver for T_{VW}/D_{MAX} variation found that D_{MAX} is more important (Pittermann *et al.* 2006; Sperry *et al.* 2006), thereby reducing the relevance of conduit wall thickening.

Vessel grouping (V_G), the final anatomical variable in the multiple regression P_{50} model, is the only character independent from lignification, and only accounts for 17% of the variation (Fig. 4a) and 5% of the P_{88} variation. Pearson's correlation analysis shows a significant positive correlation between V_G and embolism resistance. Increased vessel connectivity safeguards all pathways in the 3D vessel network when only one vessel in a vessel multiple is embolized (Carlquist, 1984; Lens *et al.*, 2011). This can only work when the intervessel pit membranes are sufficiently thick to isolate the embolisms in a given vessel multiple at a normal drought stress level, which seems to be the case in *Arabidopsis*. If T_{PM} is too thin, greater vessel connectivity increases the probability of embolism spreading via air-seeding, potentially leading to lethal levels of hydraulic failure (Tyree and Zimmermann 2002; Loepfe *et al.*, 2007; Johnson *et al.*, 2020).

In conclusion, we found a twofold difference in stem P_{50} across the *Arabidopsis* accessions studied, with the woody mutant (*soc1 ful*) being most resistant to embolism compared to the wildtype accessions. This confirms earlier studies that found a link between increased stem lignification and increased embolism resistance in *Arabidopsis* and other lineages. However, a higher degree of stem lignification cannot functionally explain the pattern observed, and therefore has to co-evolve with traits that functionally impact P_{50} . Intervessel pit membrane thickness (T_{PM}), and to a lesser extent theoretical vessel implosion resistance ($(T_{VW}/D_{MAX})^2$), vessel wall thickness (T_V) and pit chamber depth (D_{PC}), are strongly correlated with vulnerability to embolism and contribute most to the P_{12} - P_{50} - P_{88} variation observed, making T_{PM} the main functional missing link between stem lignification and embolism resistance. Adding more accessions and performing complementary measurements related to drought tolerance in stems, leaves and roots will undoubtedly shed more light into the complex mechanism that this short-lived, herbaceous model species has developed in order to cope with periods of water shortage.

ACKNOWLEDGEMENTS

We thank Gaëlle Capdeville, Regis Burlett, Anne-Isabelle Gravel and Laurent Lamarque for technical support. We also acknowledge the statistical support of Pablo Cisneros Araujo.

FUNDING

This work is funded by a PhD scholarship awarded to AT from the Institute for the Promotion of Teaching Science and Technology (IPST), Thailand, and by the Dutch Research Council NWO (grant number ALWOP.488).

LITERATURE CITED

- Adams HD, Zeppel MJB, Anderegg WRL, et al. 2017.** A multi-species synthesis of physiological mechanisms in drought-induced tree mortality. *Nature Ecology & Evolution* **1**: 1285–1291.
- Agusti J, Herold S, Schwarz M, et al. 2011.** Strigolactone signaling is required for auxin-dependent stimulation of secondary growth in plants. *Proceedings of the National Academy of Sciences* **108**: 20242–20247.
- Ahmad HB, Lens F, Capdeville G, Burlett R, Lamarque LJ, Delzon S. 2018.** Intraspecific variation in embolism resistance and stem anatomy across four sunflower (*Helianthus annuus* L.) accessions. *Physiologia Plantarum* **163**: 59–72.
- Allen CD, Macalady AK, Chenchouni H, et al. 2010.** A global overview of drought and heat-induced tree mortality reveals emerging climate change risks for forests. *Forest Ecology and Management* **259**: 660–684.
- Anderegg WRL, Klein T, Bartlett M, et al. 2016.** Meta-analysis reveals that hydraulic traits explain cross-species patterns of drought-induced tree mortality across the globe. *Proceedings of the National Academy of Sciences* **113**: 5024–5029.
- Asseng S, Ewert F, Martre P, et al. 2015.** Rising temperatures reduce global wheat production. *Nature Climate Change* **5**: 143–147.
- Awad H, Herbette S, Brunel N, et al. 2012.** No tradeoff between hydraulic and mechanical properties in several transgenic poplars modified for lignins metabolism. *Environmental and Experimental Botany* **77**: 185–195.
- Bac-Molenaar JA, Granier C, Keurentjes JJB, Vreugdenhil D. 2016.** Genome-wide association mapping of time-dependent growth responses to moderate drought stress in *Arabidopsis*. *Plant, Cell & Environment* **39**: 88–102.
- Billon LM, Blackman CJ, Cochard H, et al. 2020.** The droughtbox: a new tool for phenotyping residual branch conductance and its temperature dependence during drought. *Plant, Cell & Environment* **43**: 1–11.
- Bouche PS, Larter M, Domec J-C, et al. 2014.** A broad survey of hydraulic and mechanical safety in the xylem of conifers. *Journal of Experimental Botany* **65**: 4419–4431.
- Bourbia I, Carins- Murphy MR, Gracie A, Brodribb TJ. 2020.** Xylem cavitation isolates leaky flowers during water stress in pyrethrum. *New Phytologist*: nph.16516.
- Brackmann K, Qi J, Gebert M, et al. 2018.** Spatial specificity of auxin responses coordinates wood formation. *Nature Communications* **9**: 875.
- Brodribb TJ. 2009.** Xylem hydraulic physiology: the functional backbone of terrestrial plant productivity. *Plant Science* **177**: 245–251.
- Brodribb TJ, Bienaimé D, Marmottant P. 2016.** Revealing catastrophic failure of leaf networks under stress. *Proceedings of the National Academy of Sciences* **113**: 4865–4869.

Brodrribb TJ, Cochard H. 2009. Hydraulic failure defines the recovery and point of death in water-stressed conifers. *Plant Physiology* **149**: 575–584.

Brodrribb T, Hill RS. 1999. The importance of xylem constraints in the distribution of conifer species. *New Phytologist* **143**: 365–372.

Brodrribb TJ, Powers J, Cochard H, Choat B. 2020. Hanging by a thread? forests and drought. *Science* **368**: 261–266.

Brown HR. 2013. The Theory of the Rise of Sap in Trees: Some Historical and Conceptual Remarks. *Physics in Perspective* **15**: 320–358.

Carlquist S. 1984. Vessel grouping in dicotyledon wood: significance and relationship to imperforate tracheary elements. *Aliso* **10**: 505–525.

Chaffey N, Cholewa E, Regan S, Sundberg B. 2002. Secondary xylem development in *Arabidopsis*: a model for wood formation. *Physiologia Plantarum* **114**: 594–600.

Choat B, Brodrribb TJ, Brodersen CR, Duursma RA, López R, Medlyn BE. 2018. Triggers of tree mortality under drought. *Nature* **558**: 531–539.

Choat B, Jansen S, Brodrribb TJ, et al. 2012. Global convergence in the vulnerability of forests to drought. *Nature* **491**: 752–755.

Cochard H. 2002. A technique for measuring xylem hydraulic conductance under high negative pressures. *Plant, Cell and Environment* **25**: 815–819.

Cochard H. 2006. Cavitation in trees. *Comptes Rendus Physique* **7**: 1018–1026.

Cochard H, Badel E, Herbette S, Delzon S, Choat B, Jansen S. 2013. Methods for measuring plant vulnerability to cavitation: a critical review. *Journal of Experimental Botany* **64**: 4779–4791.

Cochard H, Damour G, Bodet C, Tharwat I, Poirier M, Améglio T. 2005. Evaluation of a new centrifuge technique for rapid generation of xylem vulnerability curves. *Physiologia Plantarum* **124**: 410–418.

Corso D, Delzon S, Lamarque LJ, et al. 2020. Neither xylem collapse, cavitation, or changing leaf conductance drive stomatal closure in wheat. *Plant, Cell & Environment* **43**: 854–865.

Dixon HH, Joly J. 1895. On the ascent of sap. *Philosophical Transactions of the Royal Society of London. B* **186**: 563–576.

Dória LC, Meijs C, Podadera DS, et al. 2019. Embolism resistance in stems of herbaceous Brassicaceae and Asteraceae is linked to differences in woodiness and precipitation. *Annals of Botany* **124**: 1–14.

Dória LC, Podadera DS, Arco M, et al. 2018. Insular woody daisies (*Argyranthemum*, Asteraceae) are more resistant to drought- induced hydraulic failure than their herbaceous relatives (R Oliveira, Ed.). *Functional Ecology* **32**: 1467–1478.

Gleason SM, Blackman CJ, Cook AM, Laws CA, Westoby M. 2014. Whole-plant capacitance, embolism resistance and slow transpiration rates all contribute to longer desiccation times in woody angiosperms from arid and wet habitats. *Tree Physiology* **34**: 275–284.

Gleason SM, Westoby M, Jansen S, et al. 2016. On research priorities to advance understanding of the safety–efficiency tradeoff in xylem: a response to Bittencourt et al.’s (2016) comment ‘On xylem hydraulic efficiencies, wood space- use and the safety–efficiency tradeoff.’ *New Phytologist* **211**: 1156–1158.

Hacke UG, Jansen S. 2009. Embolism resistance of three boreal conifer species varies with pit structure. *New Phytologist* **182**: 675–686.

Hacke UG, Sperry JS, Pockman WT, Davis SD, McCulloh KA. 2001. Trends in wood density and structure are linked to prevention of xylem implosion by negative pressure. *Oecologia* **126**: 457–461.

Hamann T, Smets E, Lens F. 2011. A comparison of paraffin and resin-based techniques used in bark anatomy. *TAXON* **60**: 841–851.

Hoffmann WA, Marchin RM, Abit P, Lau OL. 2011. Hydraulic failure and tree dieback are associated with high wood density in a temperate forest under extreme drought: tree responses to severe drought. *Global Change Biology* **17**: 2731–2742.

Holloway-Phillips M-M, Brodribb TJ. 2011. Minimum hydraulic safety leads to maximum water-use efficiency in a forage grass. *Plant, Cell & Environment* **34**: 302–313.

Jacobsen AL, Agenbag L, Esler KJ, Pratt RB, Ewers FW, Davis SD. 2007. Xylem density, biomechanics and anatomical traits correlate with water stress in 17 evergreen shrub species of the Mediterranean-type climate region of South Africa. *Journal of Ecology* **95**: 171–183.

Jacobsen AL, Ewers FW, Pratt RB, Paddock WA, Davis SD. 2005. Do xylem fibers affect vessel cavitation resistance? *Plant Physiology* **139**: 546–556.

Jansen S, Choat B, Pletsers A. 2009. Morphological variation of intervessel pit membranes and implications to xylem function in angiosperms. *American Journal of Botany* **96**: 409–419.

Johnson KM, Brodersen C, Carins-Murphy MR, Choat B, Brodribb TJ. 2020. Xylem embolism spreads by single-conduit events in three dry forest angiosperm stems. *Plant Physiology* **184**: 212–222.

Kaack L, Altaner CM, Carmesin C, et al. 2019. Function and three-dimensional structure of intervessel pit membranes in angiosperms: a review (LA Donaldson, Ed.). *IAWA Journal* **40**: 673–702.

Karami O, Rahimi A, Khan M, et al. 2020. A suppressor of axillary meristem maturation promotes longevity in flowering plants. *Nature Plants* **6**: 368–376.

Khurmatov KK. 1982. Heterogeneity of natural populations of *Arabidopsis thaliana* (pamiro-alay) in the flowering time. *Arabidopsis Inf Serv.* **19**: 62–66.

Ko J-H, Han K-H, Park S, Yang J. 2004. Plant body weight-induced secondary growth in *Arabidopsis* and its transcription phenotype revealed by whole-transcriptome profiling. *Plant Physiology* **135**: 1069–1083.

Koornneef M, Meinke D. 2010. The development of *Arabidopsis* as a model plant. *The Plant Journal* **61**: 909–921.

Lamarque LJ, Delzon S, Toups H, et al. 2020. Over- accumulation of abscisic acid in transgenic tomato plants increases the risk of hydraulic failure. *Plant, Cell & Environment* **43**: 548–562.

Larter M, Brodribb TJ, Pfautsch S, Burlett R, Cochard H, Delzon S. 2015. Extreme aridity pushes trees to their physical limits. *Plant Physiology* **168**: 804–807.

Lens F, Picon-Cochard C, Delmas CE, et al. 2016. Herbaceous angiosperms are not more vulnerable to drought-induced embolism than angiosperm trees. *Plant Physiology*: 661–667.

Lens F, Smets E, Melzer S. 2012. Stem anatomy supports *Arabidopsis thaliana* as a model for insular woodiness: Letter. *New Phytologist* **193**: 12–17.

Lens F, Sperry JS, Christman MA, Choat B, Rabaey D, Jansen S. 2011. Testing hypotheses that link wood anatomy to cavitation resistance and hydraulic conductivity in the genus *Acer*. *New Phytologist* **190**: 709–723.

Lens F, Tixier A, Cochard H, Sperry JS, Jansen S, Herbette S. 2013. Embolism resistance as a key mechanism to understand adaptive plant strategies. *Current Opinion in Plant Biology* **16**: 287–292.

Li S, Lens F, Espino S, et al. 2016. Intervessel pit membrane thickness as a key dominant of embolism resistance in angiosperm xylem. *IAWA Journal* **37**: 152–171.

Li Y, Sperry JS, Shao M. 2009. Hydraulic conductance and vulnerability to cavitation in corn (*Zea mays* L.) hybrids of differing drought resistance. *Environmental and Experimental Botany* **66**: 341–346.

Lima TRA, Carvalho ECD, Martins FR, et al. 2018. Lignin composition is related to xylem embolism resistance and leaf life span in trees in a tropical semiarid climate. *New Phytologist* **219**: 1252–1262.

Lobin W. 1983. The occurrence of *Arabidopsis thaliana* in the Cape Verde Islands. *Arab Info Ser* **20**: 119–123.

Loepfe L, Martinez-Vilalta J, Piñol J, Mencuccini M. 2007. The relevance of xylem network structure for plant hydraulic efficiency and safety. *Journal of Theoretical Biology* **247**: 788–803.

Lucas WJ, Groover A, Lichtenberger R, et al. 2013. The plant vascular system: evolution, development and functions^F. *Journal of Integrative Plant Biology* **55**: 294–388.

Maherali H, Pockman WT, Jackson RB. 2004. Adaptive variation in the vulnerability of woody plants to xylem cavitation. *Ecology* **85**: 2184–2199.

- Martin-StPaul N, Delzon S, Cochard H. 2017.** Plant resistance to drought depends on timely stomatal closure (H Maherali, Ed.). *Ecology Letters* **20**: 1437–1447.
- Melzer S, Lens F, Gennen J, Vanneste S, Rohde A, Beeckman T. 2008.** Flowering-time genes modulate meristem determinacy and growth form in *Arabidopsis thaliana*. *Nature Genetics* **40**: 1489–1492.
- Monda K, Negi J, Iio A, et al. 2011.** Environmental regulation of stomatal response in the *Arabidopsis* Cvi-0 ecotype. *Planta* **234**: 555–563.
- Nieminen KM, Kauppinen L, Helariutta Y. 2004.** A weed for wood? *Arabidopsis* as a genetic model for xylem development. *Plant Physiology* **135**: 653–659.
- Nolf M, Pagitz K, Mayr S. 2014.** Physiological acclimation to drought stress in *Solidago canadensis*. *Physiologia Plantarum* **150**: 529–539.
- Nolf M, Rosani A, Ganthaler A, Beikircher B, Mayr S. 2016.** Herb hydraulics: inter and intraspecific variation in three *Ranunculus* species. *Plant Physiology* **170**: 2085–2094.
- Pammenter NW, Van der Willigen C. 1998.** A mathematical and statistical analysis of the curves illustrating vulnerability of xylem to cavitation. *Tree Physiology* **18**: 589–593.
- Passardi F, Dobias J, Valério L, Guimil S, Penel C, Dunand C. 2007.** Morphological and physiological traits of three major *Arabidopsis thaliana* accessions. *Journal of Plant Physiology* **164**: 980–992.
- Pereira L, Domingues-Junior AP, Jansen S, Choat B, Mazzafera P. 2018.** Is embolism resistance in plant xylem associated with quantity and characteristics of lignin? *Trees* **32**: 349–358.
- Pickard WF. 1981.** The ascent of sap in plants. *Progress in Biophysics and Molecular Biology* **37**: 181–229.
- Pittermann J, Sperry JS, Wheeler JK, Hacke UG, Sikkema EH. 2006.** Mechanical reinforcement of tracheids compromises the hydraulic efficiency of conifer xylem. *Plant, Cell and Environment* **29**: 1618–1628.
- Rosenthal DM, Stiller V, Sperry JS, Donovan LA. 2010.** Contrasting drought tolerance strategies in two desert annuals of hybrid origin. *Journal of Experimental Botany* **61**: 2769–2778.
- Saha S, Holbrook NM, Montti L, Goldstein G, Cardinot GK. 2009.** Water relations of *Chusquea ramosissima* and *Merostachys clausenii* in Iguazu national park, Argentina. *Plant Physiology* **149**: 1992–1999.
- Schenk HJ, Espino S, Rich-Cavazos SM, Jansen S. 2018.** From the sap's perspective: the nature of vessel surfaces in angiosperm xylem. *American Journal of Botany* **105**: 172–185.
- Schenk HJ, Espino S, Romo DM, et al. 2017.** Xylem surfactants introduce a new element to the cohesion-tension theory. *Plant Physiology* **173**: 1177–1196.

Scholz A, Klepsch M, Karimi Z, Jansen S. 2013. How to quantify conduits in wood? *Frontiers in Plant Science* **4**: 1–11.

Skelton RP, Brodribb TJ, Choat B. 2017. Casting light on xylem vulnerability in an herbaceous species reveals a lack of segmentation. *New Phytologist* **214**: 561–569.

Somssich M. 2019. A short history of *Arabidopsis thaliana* (L.) Heynh. Columbia-0. *PeerJ Preprints* 7:e26931v5. [doi:10.7287/peerj.preprints.26931v5](https://doi.org/10.7287/peerj.preprints.26931v5).

Sperry JS. 2003. Evolution of water transport and xylem structure. *International Journal of Plant Sciences* **164**: S115–S127.

Sperry JS, Hacke UG, Pittermann J. 2006. Size and function in conifer tracheids and angiosperm vessels. *American Journal of Botany* **93**: 1490–1500.

Sperry JS, Tyree MT. 1988. Mechanism of water stress-induced xylem embolism. *Plant Physiology* **88**: 581–587.

Steudle E. 2001. The cohesion-tension mechanism and the acquisition of water by plant roots. *Annual review of plant physiology and plant molecular biology* **52**: 847–875.

Stiller V. 2002. Cavitation fatigue and its reversal in sunflower (*Helianthus annuus* L.). *Journal of Experimental Botany* **53**: 1155–1161.

Toen MPM, Davila Olivas NH, Kloth KJ, et al. 2017. Genetic architecture of plant stress resistance: multi-trait genome-wide association mapping. *New Phytologist* **213**: 1346–1362.

Tixier A, Cochard H, Badel E, Dusotoit-Coucaud A, Jansen S, Herbette S. 2013. *Arabidopsis thaliana* as a model species for xylem hydraulics: does size matter? *Journal of Experimental Botany* **64**: 2295–2305.

Trontin C, Tisné S, Bach L, Loudet O. 2011. What does *Arabidopsis* natural variation teach us (and does not teach us) about adaptation in plants? *Current Opinion in Plant Biology* **14**: 225–231.

Trueba S, Pouteau R, Lens F, et al. 2017. Vulnerability to xylem embolism as a major correlate of the environmental distribution of rain forest species on a tropical island. *Plant, Cell & Environment* **40**: 277–289.

Tyree MT, Fiscus EL, Wulschleger SD, Dixon MA. 1986. Detection of xylem cavitation in corn under field conditions. *Plant Physiology* **82**: 597–599.

Tyree MT, Zimmermann MH. 2002. *Xylem structure and the ascent of sap*. Berlin, Heidelberg: Springer Berlin Heidelberg.

Urli M, Porte AJ, Cochard H, Guengant Y, Burlett R, Delzon S. 2013. Xylem embolism threshold for catastrophic hydraulic failure in angiosperm trees. *Tree Physiology* **33**: 672–683.

Venturas MD, Sperry JS, Hacke UG. 2017. Plant xylem hydraulics: What we understand, current research, and future challenges: Plant xylem hydraulics. *Journal of Integrative Plant Biology* **59**: 356–389.

Voltaire F, Lens F, Cochard H, et al. 2018. Embolism and mechanical resistances play a key role in dehydration tolerance of a perennial grass *Dactylis glomerata* L. *Annals of Botany* **122**: 325–336.

Wheeler JK, Sperry JS, Hacke UG, Hoang N. 2005. Inter-vessel pitting and cavitation in woody Rosaceae and other vesselless plants: a basis for a safety versus efficiency tradeoff in xylem transport. *Plant, Cell and Environment* **28**: 800–812.

Wheeler TD, Stroock AD. 2008. The transpiration of water at negative pressures in a synthetic tree. *Nature* **455**: 208–212.

Zhang Y, Carmesin C, Kaack L, et al. 2020. High porosity with tiny pore constrictions and unbending pathways characterize the 3D structure of intervessel pit membranes in angiosperm xylem. *Plant, Cell & Environment* **43**: 116–130.

Zhang Y-J, Rockwell FE, Graham AC, Alexander T, Holbrook NM. 2016. Reversible leaf xylem collapse: a potential “circuit breaker” against cavitation. *Plant Physiology* **172**: 2261–2274.

Accepted Manuscript

FIG. 1 Stem P_{50} is significantly different across *A. thaliana* accessions. (a) mean vulnerability curves (VCs) for each accession presents the percentage loss of conductivity (PLC) as a function of xylem pressure (MPa). The dotted line shows 50% loss of conductivity (P_{50}). Shaded bands represent standard errors based on ca. 10 VCs per accession.; (b) boxplot showing P_{50} distribution and variation within and between accessions (p-value = 0.05).

FIG. 2 Illustration of growth form and cross-sections of inflorescence stems of Col-0 (left, 57 days after sowing) and Cvi (right, 57 days after sowing). (a, b) growth form; (c, d) transmission electron microscope images of intervessel pit membranes (arrows); (e, f) light microscope images of the cross-section at the middle part of inflorescence stems; (g, h) light microscope images of the cross-section at the basal part of inflorescence stems. Scale bars represent 1 μm (c-d), or 500 μm (e-h).

FIG. 3 Illustration of growth form and cross-sections of inflorescence stems of Sha (left, 57 days after sowing) and *soc1 ful* (right, 80 days after sowing). (a, b) growth form; (c, d) transmission electron microscope images of intervessel pit membranes (arrows); (e, f) light microscope images of the cross-section at the middle part of inflorescence stems, the double-pointed arrow shows the wood cylinder; (g, h) light microscope images of the cross-section at the basal part of inflorescence stems, the double-pointed arrow shows the wood cylinder. Scale bars represent 1 μm (c-d), 500 μm (e-h).

FIG. 4 The relative importance and correlations of intervessel pit membrane thickness and theoretical vessel implosion resistance to P_{50} (a) Relative importance of P_{50} variation is mainly explained by intervessel pit membrane thickness (T_{PM}) and theoretical vessel implosion resistance $(T_{VW}/D_{MAX})^2$ based on R^2 contribution averaged over orderings among regressors; (b) negative correlation between thickness of intervessel pit membrane (T_{PM}) and P_{50} ; (c) negative correlation between theoretical vessel implosion resistance $(T_{VW}/D_{MAX})^2$ and P_{50} . Colours and styles refer to the accession studied: Col-0 (blue-filled square), Cvi (red-filled circle), Sha (green-filled triangle) and *soc1 ful* (brown-filled diamond).

Table 1 List with the anatomical characters measured with reference to their acronyms, definitions, calculations, microscope techniques, and units.

Acronyms	Definition	Calculation	Number of measurements	Unit	Technique
A_F	Fibre cell area	Area of single xylem fibre in cross-section	Min. 30 fibres	μm^2	LM
A_{FL}	Fibre lumen area	Area of single xylem fibre lumen in cross-section	Min. 30 fibres	μm^2	LM
A_{FW}	Fibre wall area	$A_F - A_{FL}$ for the same fibre	Min. 30 fibres	μm^2	LM
A_{LIG}	Lignified stem area	Total xylem area + fibre caps area + lignified pith cell area in cross-section	9 stems per accession	mm^2	LM
A_{PITH}	Pith area	Total pith area in cross-section	9 stems per accession	mm^2	LM
A_S	Total stem area	Total stem area in cross-section	9 stems per accession	mm^2	LM
D	Diameter of vessels	Equation 3	Min. 50 vessels	μm	LM
D_H	Hydraulically weighted vessel diameter	Equation 4	Min. 50 vessels	μm	LM

D_{MAX}	Maximum vessel lumen diameter	Diameter of single vessel	Min. 30 vessels	μm	LM
D_{PC}	Pit chamber depth	Distance from the relaxed pit membrane to the inner pit aperture	Min. 25 pits	μm	TEM
P_{FWFA}	Proportion of fibre wall area per fibre cell area	A_{FW}/A_F for the same fibre; a measure of xylem fibre wall thickness	Min. 30 fibres	-	LM
P_{LIG}	Proportion of lignified area per total stem area	A_{LIG}/A_S	9 stems per accession	-	LM
T_{PM}	Intervessel pit membrane thickness	Thickness of intervessel pit membrane measured at its thickest point	Min. 25 measurements	μm	TEM
T_V	Vessel wall thickness	Thickness of a single vessel wall	Min. 30 Vessels	μm	LM
T_{VW}/D_{MAX}	Thickness-to-span ratio of vessels	Double intervessel wall thickness divided by the maximum diameter of the largest vessel	Min. 30 measurements	μm	LM

$(T_{VW}/D_{MAX})^2$	Theoretical vessel implosion resistance	$(T_{VW}/D_{MAX})^2$	Min. 30 measurements	-	LM
V_D	Vessel density	Number of vessels per mm^2	Min. 5 measurements	No. of vessels/ mm^2	LM
V_G	Vessel grouping index	Ratio of total number of vessels to total number of vessel groupings (incl. solitary and grouped vessels)	Min. 50 vessel groups	-	LM

Table 2 The best multiple regression model, based on AIC scores, of anatomical features explaining P_{50} variation in stems of the four *Arabidopsis thaliana* accessions studied.

Predictors	Estimate	Std. Error	z value	Pr (> z)
(Intercept)	0.901	0.315	2.858	0.004262
T_{PM}	-10.896	2.035	-5.356	8.522E-08***
$(T_{VW}/D_{MAX})^2$	-35.174	10.927	-3.219	0.001287**
T_V	-0.516	0.239	-2.163	0.031*
V_G	-0.280	0.183	-1.529	0.126

T_{PM} = intervessel pit membrane thickness; $(T_{VW}/D_{MAX})^2$ = theoretical vessel implosion resistance; T_V = vessel wall thickness; V_G = vessel grouping index; *** p-value < 0.001; ** p-value < 0.01; *p-value < 0.05

Figure 1

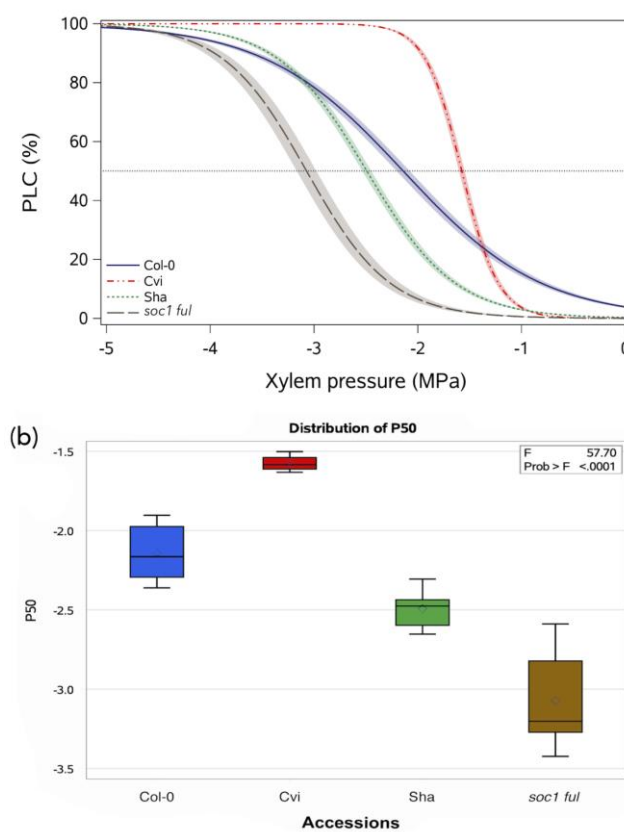


Figure 2

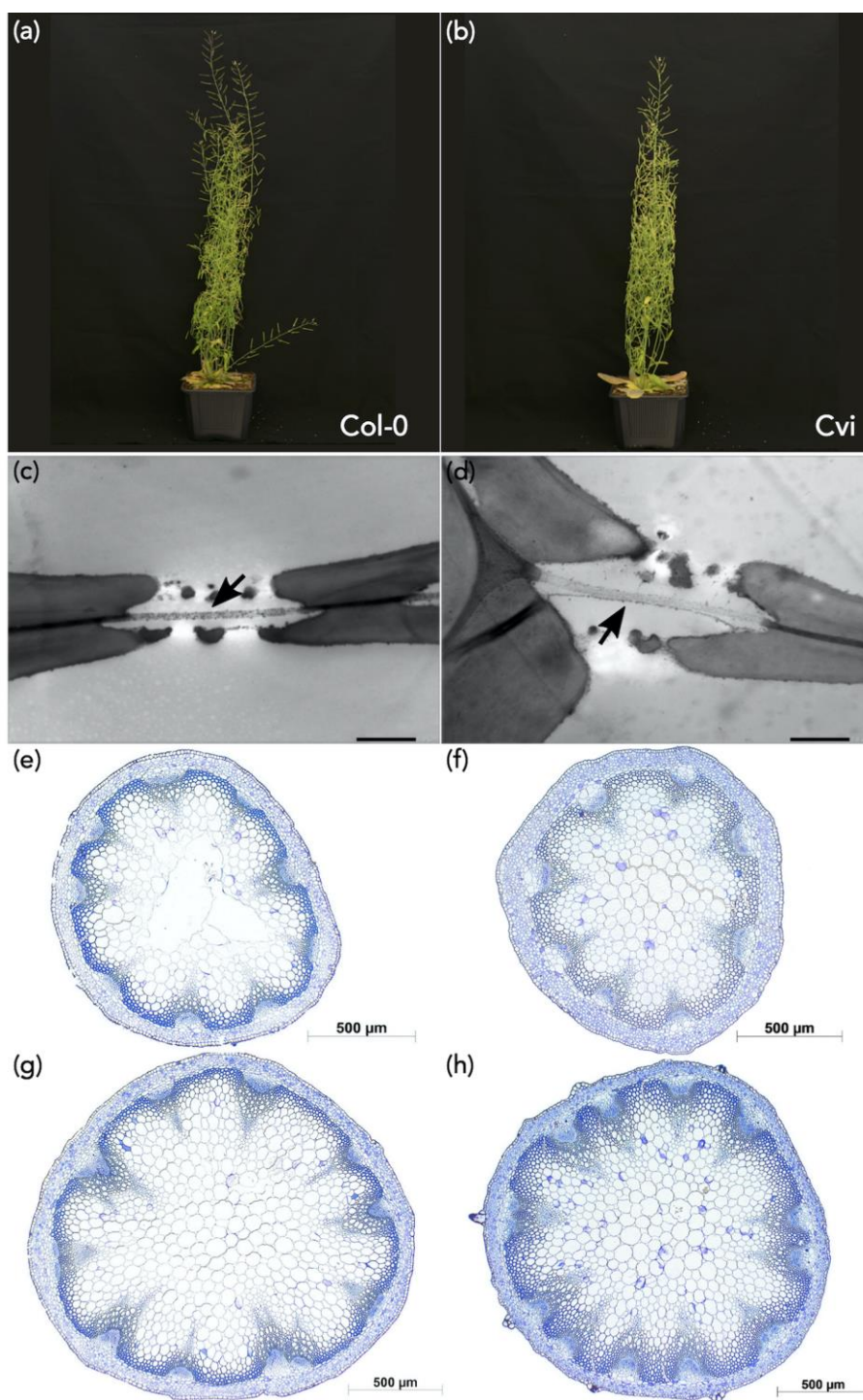


Figure 3

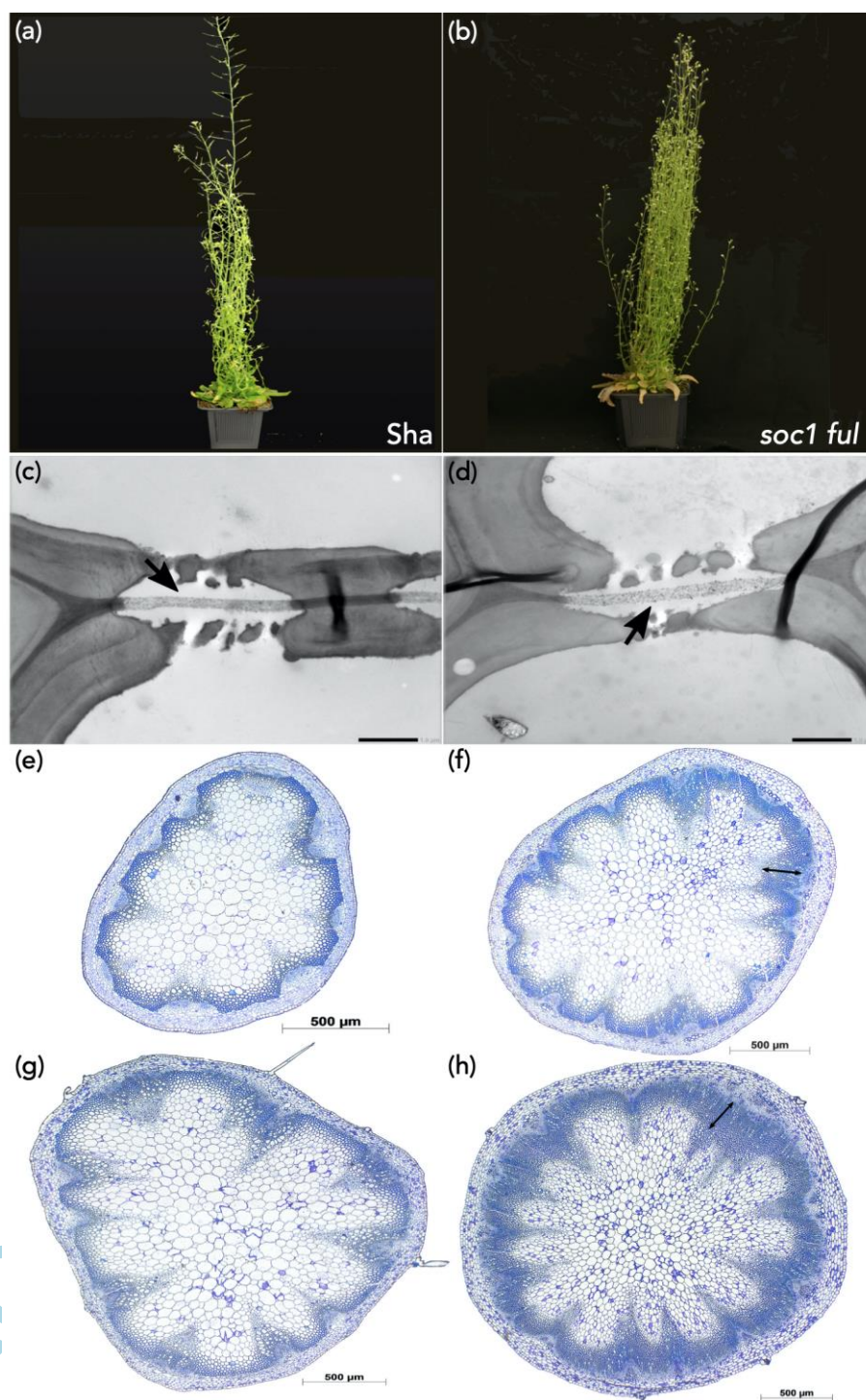


Figure 4

